Dynamic Stability of an Isentropic Shear Layer in a Statically Stable Medium

EARL E. GOSSARD

Wave Propagation Laboratory, NOAA/ERL, Boulder, Colo. 80302

(Manuscript received 19 July 1973, in revised form 1 November 1973)

ABSTRACT

Two theoretical models of shear layers in the atmosphere are examined. The conditions for their dynamic stability are found and their predictions of wavelength to layer-thickness ratio are compared with classical models and with available observational data. Although the models are only rigorously applicable to incompressible fluids, it is suggested that they also represent conditions in the atmosphere, and clear-air returns published by Katz from the high-power pulse radar at Wallops Island are especially emphasized. Model 2 appears to be able to account for the narrow band characteristic of many of the observed events and also to explain better than other models the observed wavelength to layer-thickness ratios.

1. Background

The wave equation for small perturbations of a statically stable, incompressible fluid undergoing shear is [see e.g., Taylor, 1931, Eq. (6)]

$$\frac{d^2W(z)}{dz^2}+\left[\frac{N^2}{(u_0-C)^2}-k^2-\frac{u_0''}{(u_0-C)}-\frac{2\Gamma u_0'}{u_0-C}-\Gamma^2\right]W(z)=0. \quad (1)$$

In the above equation $W=[\rho_0(z)/\rho_s]^{\frac{1}{2}}w$, where w is the vertical velocity perturbation, ρ_0 the ambient density of the fluid, and ρ_s the density at some reference height that may be arbitrarily chosen within each layer. This transformation replaces the more common transformation of variables which only involves the factor $(\rho_0)^{\frac{1}{2}}$, and it retains the dimensions and approximate magnitudes of the variables. We have chosen to use the notation of Eckart (1960), for the Väisälä-Brunt frequency N and for $\Gamma=(g/2c_s^2)(1-N^2c_s^2/g^2)$. Since the sound velocity c_s for an incompressible fluid is infinite, $\Gamma=-N^2/2g$. Primes indicate height differentiation of the ambient velocity u_0 of the fluid. The phase velocity C is defined to be σ/k where the solutions in x and t are of the form $\exp i(kx-\sigma t)$. The influence of compressibility on atmospheric stratification can be included in Eq. (1) by expressing N and Γ in terms of potential temperature instead of density, but in applying it to the atmosphere it is required that terms in C/c_s be negligible and the acoustic solutions are therefore lost from the model.

In the following, Eq. (1) will be considered to apply to the atmosphere. Then $N^2=(g/\theta)\partial\theta/\partial z$ where θ is potential temperature. Furthermore, we will assume $u_0''=0$ (linear profile) and adopt a classical approximation that neglects the terms involving Γ. In the earth's atmosphere Γ is very small, being of the order of $g/2c_s^2$, since the dimensionless number $N^2c_s^2/g^2$ is always fractional. For an incompressible fluid, Γ is precisely zero if $N=0$, so under those conditions (1) is just

$$\frac{d^2W(z)}{dz^2}-k^2W(z)=0, \quad (2)$$

with solutions which are some combination of terms of the form

$$W=W_0e^{-kz}. \quad (3)$$

In order to make the argument that (2) is applicable in the compressible atmosphere we must justify the neglect of $2\Gamma u_0'/[u_0(z)-C]$ compared with k^2 even when $u_0(z)\to C$. If we are just concerned with the neutral curves, this is most easily done by permitting C to have a small imaginary component, i.e., consider conditions of some instability. Except for the effect of compressibility on stratification, our model will be treated as incompressible, and while its applicability to the atmosphere is suggested, the precise conditions for its justification are not pursued further. The fact that instability structures similar to those seen in the atmosphere are also found in the oceans implies that compressibility is not the primary consideration. However, since the atmosphere is more accessible to observation than the oceans, data to check the models come mostly from the atmosphere.

Eq. (2) has been used by many investigators, including Rayleigh, Kelvin, Taylor and Goldstein, to study problems in shear flow. In particular, Rayleigh (1894) examined the problem of the stability of a homogeneous fluid undergoing shear. Kelvin (1880) described the shape of the streamlines near the level where $C=u_0$, deducing the now famous "Kelvin cat's

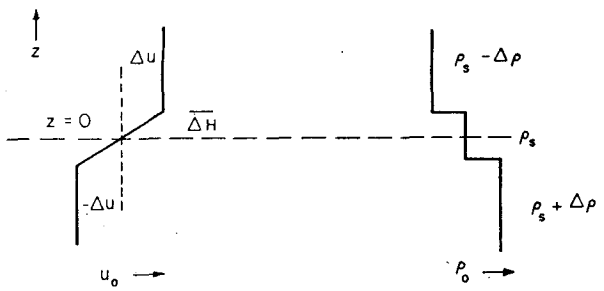

FIG. 1. Goldstein's three-layer model.

eye" pattern. Taylor (1931) and Goldstein (1931) examined several multilayer models; one is shown schematically in Fig. 1. Of course, the value of these models arose from the fact that simple solutions such as Eq. (3) could be assumed. When the dynamic and kinematic boundary conditions at the layer boundaries were satisfied, eigenvalue equations for the model were obtained which were then examined to determine the stability of perturbed flows. Models such as that in Fig. 1 were not physically realistic, but were useful in providing insight. For example, they demonstrated the importance of layer thickness on shear wave instability.

On the other hand, a model with no shear in which $N\neq 0$ has the wave equation

$$\frac{d^2W}{dz^2}-k^2\left(1-\frac{N^2}{\omega^2}\right)W=0, \tag{4}$$

where, in general,

$$\omega=k[C-u_0(z)], \tag{4a}$$

but in the shearless model u_0 is constant.

Like Eq. (2), this equation has simple solutions, i.e. of the form

$$W=W_0\exp\{-k[1-(N^2/\omega^2)]^{\frac{1}{2}}z\}. \tag{5}$$

Unlike the Taylor/Goldstein model of Fig. 1, this "no shear" model can include the static stability (in terms of N) in all layers of the model shown in Fig. 2. It was treated by Gossard and Munk (1954) who used it to analyze gravity waves in the lower atmosphere in Southern California. They found the eigenvalue equation

$$\gamma_2\,\mathrm{ctnh}(2\gamma_2\Delta H)=\frac{-\gamma_2^2-\gamma_1\gamma_3\,\mathrm{ctnh}(\gamma_1 H)}{\gamma_1\,\mathrm{ctnh}(\gamma_1 H)+\gamma_3}, \tag{6}$$

where $\gamma=k(1-N^2/\omega^2)^{\frac{1}{2}}$ and the subscripts on γ go with those on N. For a model in which $H=\infty$ and $N_1=N_3=N$, Eq. (6) becomes

$$\mathrm{ctnh}2\gamma_2\Delta H=-\frac{\gamma^2+\gamma_2^2}{2\gamma\gamma_2}. \tag{6a}$$

For models of interest, N_1 or N_2 are greater than ω so that γ_1, γ_2, or both, are pure imaginary. If wind shear is included in a model like that of Fig. 2, waves generated within the region of shear are either unstable or cannot exist if their phase velocity is anywhere equal to the wind speed (e.g., Scorer, 1951). Much effort has gone into the analysis of models with wind shear across such stable layers in an effort to determine the range of initial instability and the most unstable wavenumber at the onset of instability. We mention recent papers such as Miles and Howard (1964) who analyzed a model with profiles made up of linear segments, Drazin (1958) who analyzed a hyperbolic tangent wind profile and an exponential density profile, and Holmboe (1960) who analyzed profiles both of which were hyperbolic tangent in form. All such studies are mathematically difficult because of singularities at the critical level, where $C=u_0$, which require some form of solution of a hypergeometric differential equation. If the results of such analyses of the linearized equations [such as Eq. (1)] are applicable to the real atmosphere, they are likely to apply only at the onset of a disturbance when the perturbations are still very small. The whole subject of shear instability is very completely summarized by Drazin and Howard (1966).

Many of the recent results were anticipated in earlier papers by Taylor (1931), Goldstein (1931) and Sekera (1948). After examining the general (linearized) problem of the dynamic stability of an inviscid, statically stable layer under shear, Sekera concluded that billow clouds were a result of waves at a shear layer, and that they must occur at levels in the atmosphere where the static stability vanishes, i.e., an isentropic region, in order to account, within the linear theory, for the stability of their patterns. In this paper we explore isentropic models, and suggest that wavelike disturbances arising from shear wave instability tend to create such a model and steady patterns.

2. Model 1

For the models to be examined in this paper, the solutions (3) and (5) are applicable. A limiting form (i.e., $H=0$) has been used by Ramm and Warren

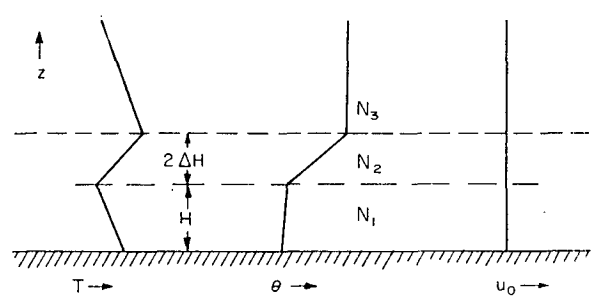

FIG. 2. Gossard-Munk three-layer model.

(1963) to examine the effect of an impulse on gravity wave generation and dispersion. Our first model is one in which a shear layer of statically neutral stability is imbedded in a medium which is otherwise statically stable and whose stability can be described by a constant Väisälä-Brunt frequency N. Then the solution applies within the shear layer and the solution [Eq. (5)] applies elsewhere. The model is shown schematically in Fig. 3, where

$$\left.\begin{aligned} &u_0=-\Delta u, && \theta=\theta_s\exp[(N_1^2/g)z], && \text{for } z<H\\ &u_0=-\Delta u+\beta(z-H), && \theta=\theta_s\exp[(N_1^2/g)H], && \text{for } H<z<H+2\Delta H\\ &u_0=\Delta u, && \theta=\theta_{H+2\Delta H}\exp[(N_3^2/g)(z-H-2\Delta H)], && \text{for } z>H+2\Delta H \end{aligned}\right\}.$$

Solutions for the various layers are of the form

$$W_1=A\sinh\gamma_1 z, \qquad z<H, \tag{7a}$$

$$W_2=B_1e^{kz}+B_2e^{-kz}, \quad H<z<H+2\Delta H, \tag{7b}$$

$$W_3=De^{-\gamma_3(z-2\Delta H)}, \qquad z>H+2\Delta H. \tag{7c}$$

The kinematic boundary condition to be satisfied at the layer interface is (for small perturbations)

$$W_1=W_2, \quad W_2=W_3,$$

and the dynamic condition is $p_1=p_2$ and $p_2=p_3$, where p is total pressure. Then

$$\frac{dp_1}{dt}=\frac{dp_2}{dt}, \quad \frac{dp_2}{dt}=\frac{dp_3}{dt};$$

therefore,

$$\left(\frac{\rho_0}{\rho_s}\right)^{\frac{1}{2}}\left(\frac{DP}{Dt}-\rho_s gW\right) \tag{8}$$

must be continuous across fluid interfaces. D/Dt is the Stokes operator

$$\frac{D}{Dt}=\frac{\partial}{\partial t}+u_0\frac{\partial}{\partial x}=-i\omega,$$

and $P=(\rho_0/\rho_s)^{-\frac{1}{2}}p'$, where p' is the pressure perturbation. The unperturbed density is ρ_0, and ρ_s the density at some reference level. For convenience the x direction is chosen to be the direction of horizontal propagation. In condition (8), it is convenient to express P in terms of W using

$$\frac{DP}{Dt}=\rho_s\frac{\omega}{k}\left[\beta W-\frac{\omega}{k}\frac{\partial W}{\partial z}\right], \tag{9}$$

where $\beta=du_0/dz=\Delta u/\Delta H$ and where ω/k is defined by Eq. (4a). Letting $\alpha=k\Delta H$, one finds from Eq. (4a) that $\omega/\beta=\sigma/\beta\pm\alpha$ in the lower (+) and upper (−) layers,

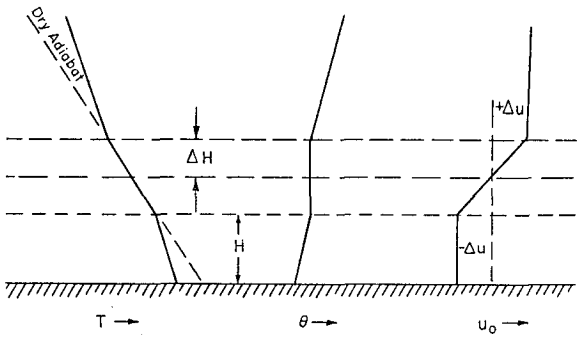

FIG. 3. Model 1.

and

$$\frac{\omega}{\beta}=\frac{\sigma}{\beta}+\alpha\left(1-\frac{z-H}{\Delta H}\right), \quad H<z<H+2\Delta H,$$

in the shear layer. Therefore,

$$\gamma_1=k\left[1-\left[\frac{N_1/\beta}{\dfrac{\sigma}{\beta}+\alpha}\right]^2\right]^{\frac{1}{2}}, \quad \gamma_3=k\left[1-\left[\frac{N_3/\beta}{\dfrac{\sigma}{\beta}-\alpha}\right]^2\right]^{\frac{1}{2}}.$$

Applying the solutions given in Eq. (7) to the condition (8), we find at the lower boundary

$$\left[\alpha_1-\alpha\frac{1-(B_2/B_1)e^{2\alpha}}{1+(B_2/B_1)e^{2\alpha}}\right]\left(\frac{C}{\Delta u}+1\right)=1, \tag{10a}$$

where we have let $\alpha_1=\gamma_1\Delta H\,\mathrm{ctnh}kH$. At the upper boundary, if we let $\alpha_3=\gamma_3\Delta H$

$$\left[\alpha\frac{1-(B_2/B_1)e^{-2\alpha}}{1+(B_2/B_1)e^{-2\alpha}}+\alpha_3\right]\left(\frac{C}{\Delta u}-1\right)=-1. \tag{10b}$$

Elimination of B_2/B_1 reveals the eigenvalue equation for the model of Fig. 3 to be

$$\left[\left(1+\frac{\alpha_1\alpha_3}{\alpha^2}\right)\tanh 2\alpha+\frac{\alpha_1+\alpha_3}{\alpha}\right]\left(\frac{\sigma}{\beta}\right)^2+\left[\left(\frac{\alpha_1-\alpha_3}{\alpha}\right)\tanh 2\alpha\right]\left(\frac{\sigma}{\beta}\right)+(2\alpha-\alpha\alpha_1-\alpha\alpha_3)$$
$$-(1+\alpha^2-\alpha_1-\alpha_3+\alpha_1\alpha_3)\tanh 2\alpha=0. \tag{11}$$

If $N=0$, the model is a three-layer homogeneous medium with the middle layer under constant shear and is one of a class of homogeneous models studied extensively by Rayleigh. Then $\alpha_3=\alpha$ and $\alpha_1=\alpha\,\mathrm{ctnh}kH$. Thus, Eq. (11) is of the form

$$a\left(\frac{\sigma}{\beta}\right)^2+b\frac{\sigma}{\beta}+c^2=0, \tag{12}$$

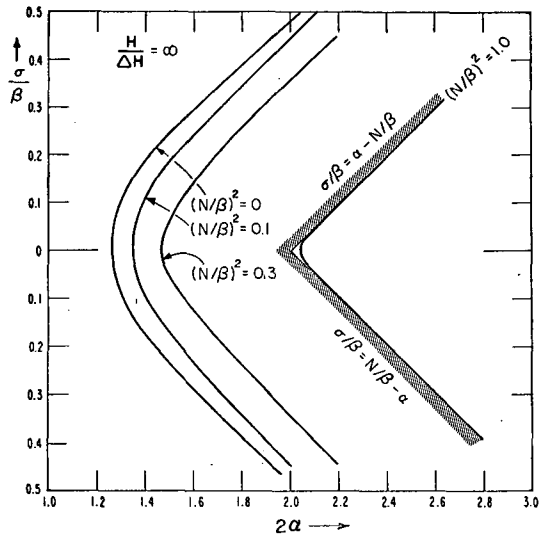

FIG. 4. Eigenvalue plots, Model 1, parametric in N^2/β^2; $H/\Delta H=\infty$. Beyond shaded lines $|\alpha\pm\sigma/\beta|<N/\beta$ and energy leaks away from layer.

where

$$\left.\begin{aligned} a&=(1+\text{ctnh}kH)(\tanh 2\alpha+1)\\ b&=(\text{ctnh}kH-1)\tanh 2\alpha\\ c&=\alpha[2-\alpha(\text{ctnh}kH+1)]\\ &\quad -[1+\alpha(\alpha-1)(1+\text{ctnh}kH)\tanh 2g]\end{aligned}\right\}.$$

The question of stability is therefore decided by the sign at b^2-4ac.

The most widely quoted result of Rayleigh is found for the model in which $H=\infty$ so that (12) reduces to

$$\left(\frac{\sigma}{\beta}\right)^2=\frac{\tanh 2\alpha}{2(\tanh 2\alpha+1)}-\alpha(1-\alpha). \tag{13}$$

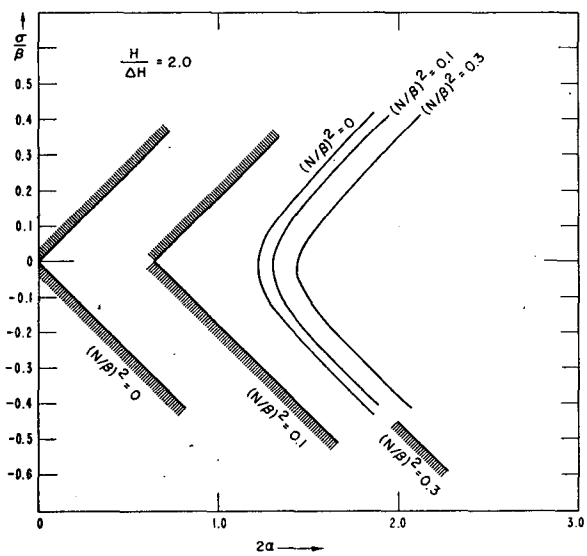

FIG. 5. Eigenvalue plots, Model 1, parametric in N^2/β^2; $H/\Delta H=2$.

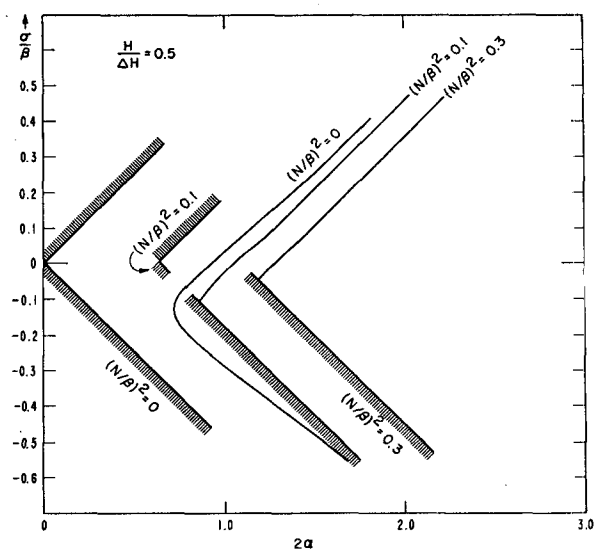

FIG. 6. Eigenvalue plots, Model 1, parametric in N^2/β^2; $H/\Delta H=0.5$.

Recalling that $\tanh 2\alpha=(1-e^{-4\alpha})/(1+e^{-4\alpha})$, one finds the Rayleigh condition for stability [σ real and $(\sigma/\beta)^2$ positive] for this model to be

$$(2\alpha-1)^2-e^{-4\alpha}>0,$$

which yields the critical ratio of wavelength to layer thickness to be

$$\frac{\lambda}{2\Delta H}=\frac{2\pi}{1.28}=4.90.$$

Rayleigh further found the most unstable wavelength [that wavelength for which $(\sigma/\beta)^2$ reaches its largest negative value] to be given by the ratio

$$\frac{\lambda}{2\Delta H}=\frac{2\pi}{0.8}=7.85.$$

At the other extreme, when $\beta=0$ (i.e., $\Delta u=0$), the "no shear" limit of Eq. (11) reduces to the Gossard-Munk equation (6) which applies to a nonhomogeneous atmosphere. If $N_2=0$, $N_1=N_3=N$, and $H=\infty$, one finds from (6) that

$$\text{ctnh}2\alpha=-\frac{\alpha^2+\alpha_0^2}{2\alpha\alpha_0},\quad \text{where}\quad \alpha_0=\alpha[1-(N/\sigma)^2]^{\frac{1}{2}}. \tag{14}$$

The plots of σ/β vs 2α, from (11), are shown in Figs. 4–6 for various values of $H/\Delta H$, assuming in all cases that $N_1=N_2=N$. The curve designated as $N^2/\beta^2=0$ is that of the Rayleigh homogeneous model [Eq. 12]. The other curves represent a generalization of the homogeneous model in which a statically neutral shear layer is imbedded in a statically stable medium.

Although N^2/β^2 is superficially like a Richardson number, N describes the stability of the medium *outside* the layer while β describes the shear *across* the layer. For values of 2α to the left of the nose of the curves, only imaginary or complex values of the frequency σ can be roots of (11) and such solutions represent unstable disturbances. On the shaded side of the straight lines, the radical in γ_1 or γ_3 becomes imaginary, i.e., $|\alpha \pm \sigma/\beta| < N/\beta$. Beyond $\sigma/\beta = \pm(N/\beta + \alpha)$, it would again become real.

The plot of σ/β vs 2α is shown parametric in $H/\Delta H$ for $N/\beta = 0$ in Fig. 7. As $H \to 0$

$$\left.\begin{aligned} a &= 1+\tanh 2\alpha \\ b &= \tanh 2\alpha \\ c &= -\alpha^2+\alpha(1-\alpha)\tanh 2\alpha \end{aligned}\right\} \text{ in Eq. (12).}$$

For this special case σ/β is real for all α and the flow is stable. This result is in accord with Rayleigh's general conclusion on "inflection point instability," since change in slope of the velocity profile has only one sign when $H=0$. The "nose" of the eigenvalue curve in this case dips in to the origin. Clearly the presence of a boundary must be considered when it is less than a wavelength from the shear layer. When it is less than 0.1 wavelength away from the layer, it is very important. The boundary effect is even more striking in Fig. 8 in which the value of $(b^2-4ac)/4a^2$ is plotted vs 2α, parametric in $H/\Delta H$. When $(b^2-4ac)/4a^2$ is negative, the frequency has an imaginary part and perturbations are unstable, growing exponentially. Its maximum negative value represents a most unstable value of 2α. The dashed curves in Fig. 8 show the real part of the ratio $C/\Delta u$ (see model) in the unstable range of $2k\Delta H$ for various values of $H/\Delta H$. When $H=\infty$, $C=0$, so the waves move with the mean wind

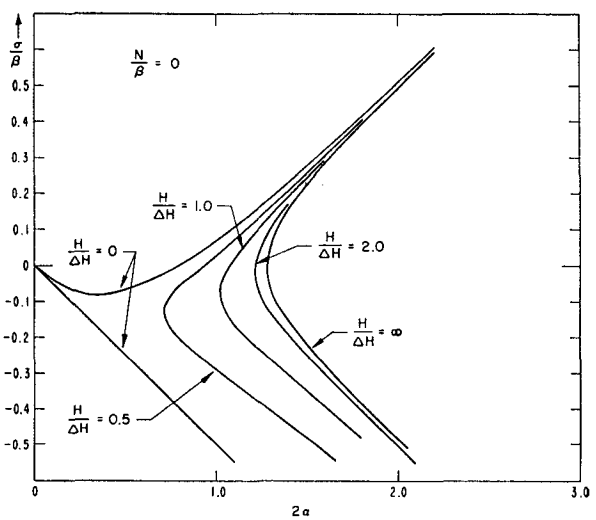

FIG. 7. Eigenvalue plots, Model 1, parametric in $H/\Delta H$, $N/\beta = 0$.

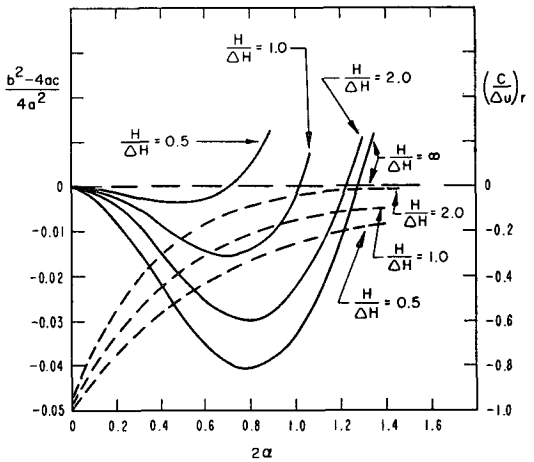

FIG. 8. Curves describing real (dashed) and imaginary (solid) components of $C/\Delta u$; parametric in $H/\Delta H$.

speed within the shear layer, i.e., zero. When $H/\Delta H$ becomes small, $C/\Delta u$ becomes significantly negative, so the waves tend to move with the wind in the lower layer.

3. Model 2

Suppose we seek a model that may be representative of intense mixing in a layer imbedded in a stable medium, and treat the model shown in Fig. 9. This model can be thought of as a generalization of the Goldstein model (Fig. 1) with a lower boundary—one in which the upper and lower layers are no longer required to be homogeneous. This model contains discontinuities in temperature (inversions) at the layer boundaries, so the boundary condition (8), taking into account the density discontinuity, requires continuity of

$$\rho_s \frac{\omega}{k}\left(\beta W - \frac{\omega}{k}\frac{\partial W}{\partial z}\right) - \rho_s g W. \tag{15}$$

Proceeding as before, applying the solutions (7), and neglecting $\Delta\rho$ compared with ρ_s (or $\Delta\theta$ compared with θ) except when it appears as a product of g, one finds

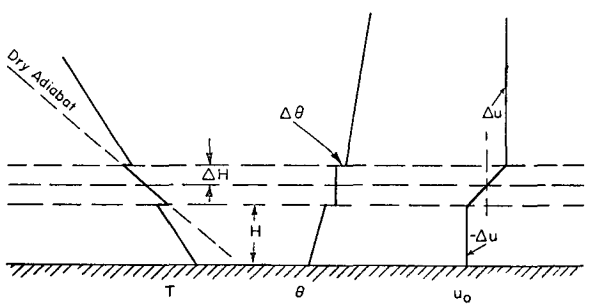

FIG. 9. Model 2.

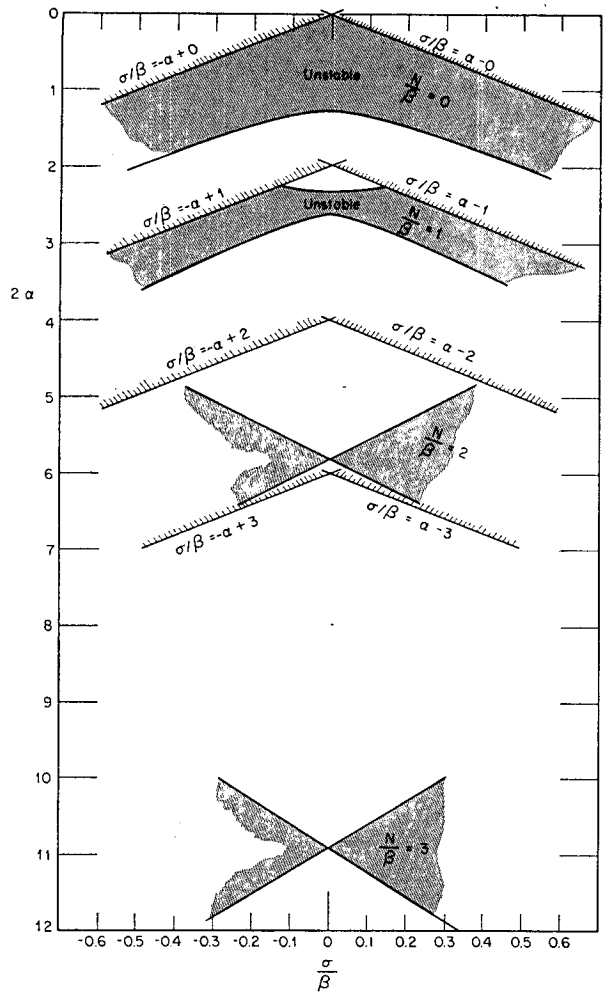

FIG. 10. Eigenvalue plots, Model 2, parametric in N^2/β^2; $H/\Delta H=\infty$.

that

$$e^{4\alpha}\left[\frac{-R_U+\left(\frac{C}{\Delta u}-1\right)^2(\alpha_3+\alpha)+\frac{C}{\Delta u}-1}{R_U+\left(\frac{C}{\Delta u}-1\right)^2(\alpha-\alpha_3)-\frac{C}{\Delta u}+1}\right]$$

$$=\left[\frac{R_L+\left(\frac{C}{\Delta u}+1\right)^2(\alpha-\alpha_1)+\frac{C}{\Delta u}+1}{-R_L+\left(\frac{C}{\Delta u}+1\right)^2(\alpha+\alpha_1)-\frac{C}{\Delta u}-1}\right],$$

where $R_{U,L}=g(\Delta\rho_s)_{U,L}\Delta H/(\rho_s\Delta u^2)$ is a kind of Richardson number for the upper (U) and lower (L) discontinuities, and $\Delta\rho_s$ is the density difference across each discontinuity. As before, we equate $\Delta\rho_s/\rho_s$ and $\Delta\theta/\theta$. Choosing the special case of $R_U=R_L=R$ and remembering that $C/\Delta u=\sigma/\alpha\beta$, it can be written

$$a\left(\frac{\sigma}{\beta}\right)^4+e\left(\frac{\sigma}{\beta}\right)^3+b\left(\frac{\sigma}{\beta}\right)^2+f\left(\frac{\sigma}{\beta}\right)+c=0, \qquad (16)$$

where

$$a=\frac{1+\alpha_1\alpha_3/\alpha_2}{\alpha^2}\tanh 2\alpha+\frac{\alpha_1+\alpha_3}{\alpha^3},$$

$$e=\frac{\alpha_1-\alpha_3}{\alpha^3}\tanh 2\alpha,$$

$$b=-\left[\frac{(R-1)(\alpha_1+\alpha_3)}{\alpha^2}+1+2(1+\alpha_1\alpha_3/\alpha^2)\right]\times\tanh 2\alpha-\frac{2}{\alpha}[R-1+(\alpha_1+\alpha_3)],$$

$$f=\frac{\alpha_1-\alpha_3}{\alpha^3}\{1-2(1+R)\}\tanh 2\alpha,$$

$$c=[(1+R-\alpha_1)(1+R-\alpha_3)+\alpha^2]\times\tanh 2\alpha+\alpha(\alpha_1+\alpha_3)-2\alpha(1+R).$$

Inspection of Fig. 9 shows that $R=N^2/\beta^2$ which greatly simplifies the parameterization of the problem when $N_1=N_3$.

When the medium in which the layer is imbedded is of neutral stability, $\alpha_1=\alpha_3=\alpha$ and the model is that shown in Fig. 1 and treated by Goldstein (1931).

The eigenvalue curves for Model 2 are shown in Fig. 10. It is apparent that as N/β increases from zero the domain of instability moves out toward larger α in a rapidly narrowing *band* of unstable wavenumbers as shown in Fig. 11 for $\sigma/\beta=0$. By the time $N/\beta=2$, the unstable range is almost pinched out and is essentially monochromatic so that wave excitation should be

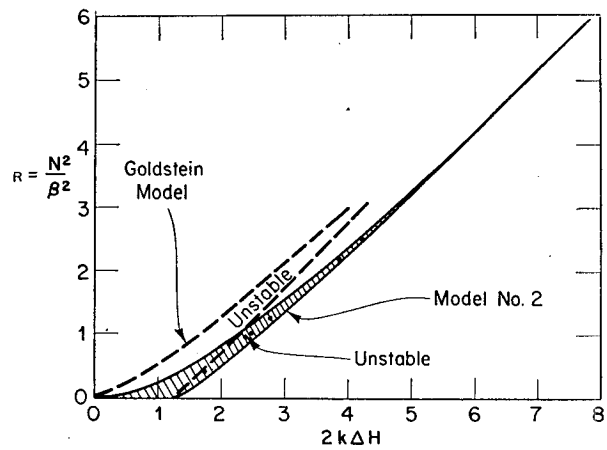

FIG. 11. Neutral curves, Model 2, for $\sigma=0$ ($C=0$). Dashed curves refer to Goldstein's model (Fig. 1). Dots are experimental values from Katz' data plotted in unstable region without regard to N/β.

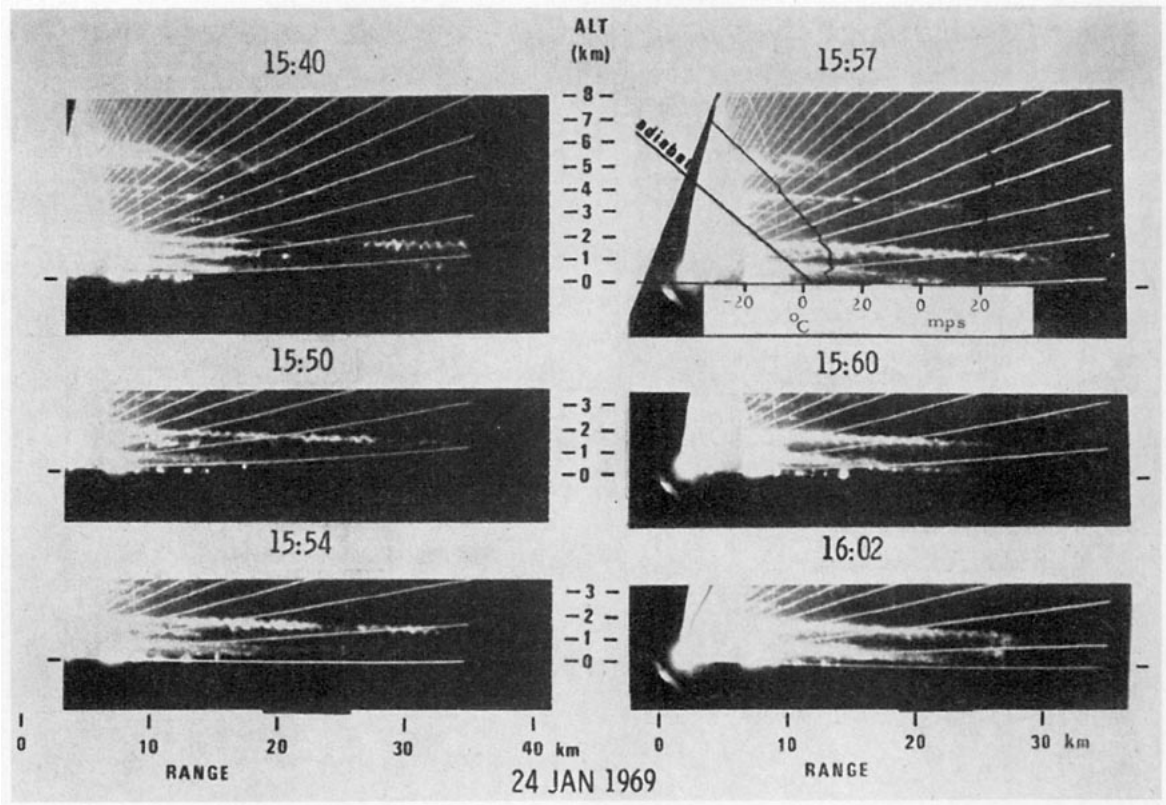

FIG. 12. Radar returns from the clear atmosphere taken from Katz (1972) for radar located at Wallops Island. The 1830 EST temperature and wind sounding at Wallops Island is shown in the 1557 EST frame of the figure. Note strongly super-adiabatic layer at about 1500 m.

highly selective in wavelength. Even for N/β as small as 1.0, the ratio of wavelength to total layer thickness ranges only from 2.4 to 2.7. However, the *magnitude* of maximum instability decreases as the band narrows, so one would expect to observe those wavelengths which lie within the region of appreciable bandwidth. Because of the spatial symmetry of the model with infinite lower and upper layers, it is natural to suppose the real part of the wave velocity C_r to be zero (and therefore $\sigma_r=0$). This can be proved in special cases; e.g., Tollmien (1935) proved that $C=u_0$ at the inflection point of a monotonic profile of velocity for a neutral disturbance in a flow of uniform density.

The above model only describes a limiting condition toward which the real atmosphere would tend when violent mixing occurs, caused perhaps by dynamic instability from shear within the medium. The extent to which the model is pertinent to the observed layer structure within the real atmosphere should be determined by observation.

4. Observations of structure on layers

A variety of models with shear layers imbedded in stably stratified media have been analyzed in recent years. For example, Drazin (1958) analyzed a model with a hyperbolic tangent wind distribution and exponential density decrease. Holmboe (1960) analyzed a model with hyperbolic tangent wind distribution and hyperbolic tangent exponent of the density distribution. Miles and Howard (1964) analyzed a three-layer model in which both wind and density were composed of linear segments, piecewise continuous. The symmetrical or nearly symmetrical models of both Holmboe (1960) and Miles and Howard (1964) give a ratio of wavelength layer thickness of about 6.5 for the "most unstable wave," and the nonsymmetrical (density) model of Drazin gives about 4.5.

Few reliable measurements exist against which to compare the various models. From acoustic sounder data and *in-situ* tower data, Emmanuel *et al.* (1972) found ratios of 5.2 and 4.0 for features in the boundary layer. From similar data on another event, Hooke *et al.* (1973) found a ratio of 3.5. Gossard *et al.* (1970) found a ratio of 3.2 for features on an elevated layer using FM-CW radar data and radiosonde sounding data. The above investigations suggest that observed ratios tend to be smaller than those implied by the major instability models for stable layers. However, all of the above observations were indirect in the sense that the horizontal scale had to be inferred from the wave velocity. Sometimes (Emmanuel *et al.*, 1972) the wave

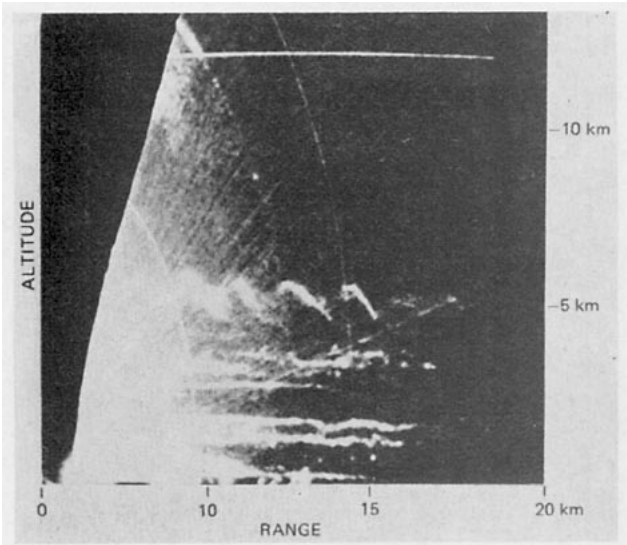

FIG. 13. Radar returns from the clear atmosphere taken from Katz (1972). Same day as in Fig. 14 but time is different.

velocity was assumed to be that of the wind at the height of the wave structure; sometimes (Hooke *et al.*, 1973) the wave velocity was deduced from the ratio of pressure perturbation to wind perturbation through the impedance equation, or (Gossard *et al.*, 1970) through the ratio of velocity perturbation components by use of polarization relations.

Table 1 is compiled from data that were published by Katz (1972). They should be more reliable than any of the earlier data referenced because the measurements of the spatial scales are direct.

Figs. 12–15 show radar returns from the clear atmosphere obtained by the powerful pulse radar of NASA at Wallops Island on a wavelength of 10 cm. From data such as these the ratio of spatial wavelength to echo layer thickness may be scaled directly. The main uncertainty concerns the question of whether the braided or wavelike features completely fill the layer and are thus a true measure of layer thickness. However, underestimation of layer thickness would *increase* the estimated ratio. The ratios so deduced are presented in Table 1.

TABLE 1. Ratios of wavelength to layer thickness from observations published by Katz (1972). Figures in parentheses are corresponding values of 2α.

Date	Figure number	Time (EST)	High layer	Middle layer	Low layer
24 Jan. 1969	14	1540	2.9(2.2)	1.5(4.2)	
		1550		2.3(2.7)	
		1554		1.6(3.9)	
		1557	4 (1.6)	1.6(3.9)	
		1560		1.5(4.2)	
24 Jan. 1969	15		2.7(2.3)		
16 May 1968	16			2.7(2.3)	
20 Dec. 1968	17				3.8(1.7)

The values of 2α are shown in parentheses in the table and are plotted in Fig. 11 (Model 2) as solid dots without regard to observed values of N^2/β^2. Reliable estimates of N^2/β^2 were impossible from the available wind sounding data, since the balloon release time was 3 hr after the radar observations. However, it is evident that the cases fall in the "narrow band" region of the graph and in a range of N^2/β^2 which is easily attained in the atmosphere. Table 1 indicates a clear tendency for the observed ratios of wavelength to layer thickness to be significantly less (average 2.3) than those predicted for the most unstable wave for shear layers in stable media. Furthermore, Model 2 provides a mechanism for strong selectivity of wavelength, as observed, whereas other models provide only weak selectivity associated with the broad peak of the neutral curves.

The sounding data for the 1830 EST (2330 GMT) balloon release on 24 January is shown in the 1557 EST frame of Fig. 12 in which the layer structure is clearest. The sounding data are too remote in time from the radar observations to provide reliable quantitative data; however, the layer structure revealed is qualitatively similar to that observed by the radar, and the presence of super-adiabatic and near-adiabatic layers in the vicinity of the radar echo layers is obvious, especially at the most periodic of the layers near 1.5 km.

In several of the references listed above, acoustic echo soundings and FM-CW radar soundings are shown which reveal structures within statically stable regions of the troposphere which appear to be unaccompanied by significantly increased temperature lapse rates according to radiosonde temperature soundings through the layers. However, such layers in the lower troposphere are thin, and these sounders cannot probe the deeper layer structure of the higher atmosphere. Since the response of the radiosonde temperature element is poor, it cannot be expected to adequately resolve such thin layers. However, the humidity element responds much faster, and the corresponding humidity distribution (or radio refractive index) invariably shows regions of small gradient in the neighborhood of thin echo layers. Since such regions of small gradient are usually (as expected) bounded by regions of large gradient, very precise matching of the height of the radiosonde with the height of layer echoes is required to establish the relationship between atmospheric structure and layer echoes. The double-echo structure often seen on sounder records may represent returns from the bounding regions of large gradient in this model. Certainly, observations using the lower tropospheric sounders do not rule out the "intense mixing" model we suggest, and the powerful pulse radars probing deeper layers of the atmosphere tend to support this model.

The observations shown in this paper tend to favor Model 2 (the limit of intense mixing in a statically

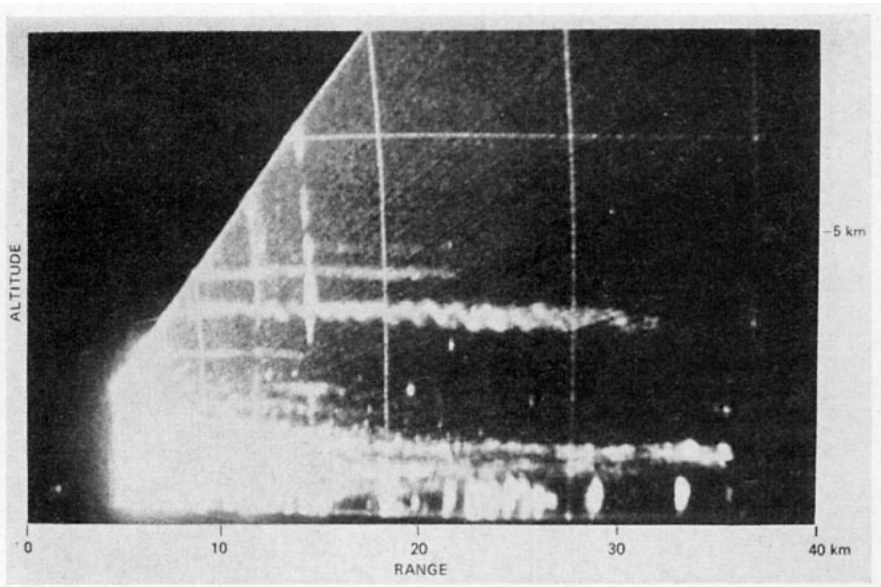

FIG. 14. Radar returns (16 May 1968) from the clear atmosphere taken from Katz (1972).

stable medium) rather than Model 1. However, Model 1 may also fairly well represent some cases of wave generation when the isentropic or nearly isentropic layer is a result of air mass dynamics or thermodynamics. In this case, the bounding inversion discontinuities might be expected to be absent as assumed in Model 1. Broad-band wave generation of this type may be the explanation of pressure oscillations of a class observed in the eastern United States which has been attributed (Madden and Claerbout, 1968) to wave generation by dynamic instability due to shear in the upper atmosphere associated with the jet stream. If the temperature lapse is nearly isentropic in such a region of shear, Model 1 may be fairly realistic.

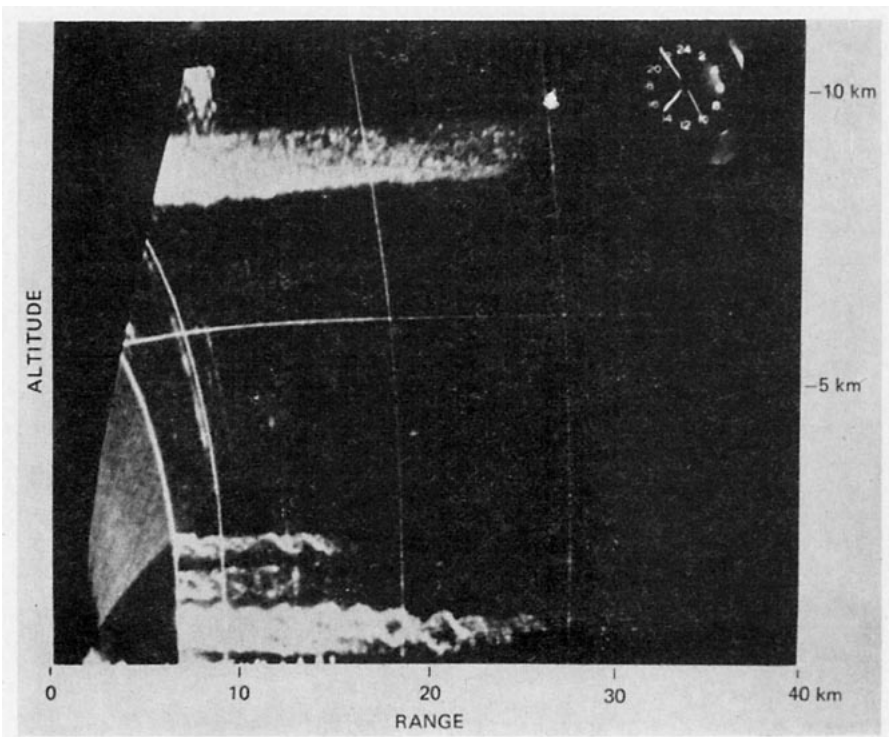

FIG. 15. Radar returns from the clear atmosphere taken from Katz (1972). Layer at about 8 km is cirrus cloud.

5. Streamlines of the flow

To find eigensolutions for the homogeneous region, either Eq. (10a) or Eq. (10b) is solved for B_2/B_1, and $C/\Delta u$ is then eliminated using Eq. (11). For an infinitely deep lower layer, and $N_1=N_3$, Eq. (10b) becomes

$$\frac{B_2}{B_1}=e^{2\alpha}\frac{(\alpha_3+\alpha)\left(\frac{C}{\Delta u}-1\right)+1}{(\alpha-\alpha_3)\left(\frac{C}{\Delta u}-1\right)-1},$$

where $\alpha_3=\gamma\Delta H$. For a homogeneous model, $\alpha=\alpha_3$ and

$$\frac{B_2}{B_1}=-e^{2\alpha}\left[2\alpha\left(\frac{C}{\Delta u}-1\right)+1\right],$$

where

$$\left(\frac{C}{\Delta u}\right)^2=\frac{(2\alpha-1)^2-e^{-4\alpha}}{4\alpha^2}, \tag{17}$$

which gives

$$\frac{B_2}{B_1}=-e^{2\alpha}\{[(2\alpha-1)^2-e^{-4\alpha}]^{\frac{1}{2}}+(1-2\alpha)\}.$$

The origin is chosen at the height where $C-u_0=0$. For the condition $C=0$, $B_2/B_1=\pm 1$, so Eq. (7b) gives

$$W_2=2B_1\cosh kz.$$

Since $C=0$, the wave system is stationary in this model and $u_0=0$ at $z=0$. Within the Boussinesq approximation (and neglecting earth rotation), $U=ik^{-1}\partial W/\partial z$. Therefore, if U_s is the amplitude of the perturbation of the horizontal wind,

$$U_2=U_s\sinh kz,$$

so the total wind in the middle layer is

$$U=\beta z+U_s e^{ikx}\sinh kz,$$

where we have now included the factor periodic in x. The streamfunction is therefore

$$\psi=\int_0^z U(z)dz=\beta\frac{z^2}{2}+\psi_s e^{ikx}\cosh kz.$$

Then, for small kz, the displacement z of the streamlines is

$$z\approx\pm(2/\beta)^{\frac{1}{2}}(\psi-\psi_s e^{ikx})^{\frac{1}{2}}.$$

When $\psi=\psi_s$, this plots as a pattern of interlacing sinusoids of wavelength 2λ centered on the height $z=0$. When $\psi>\psi_s$, the streamlines are simple sinusoids. When $\psi<\psi_s$, they are closed curves within the interlaced sinusoids. The pattern is essentially the cat's eye pattern of Kelvin.

Acknowledgments. The author expresses his appreciation to I. Katz of the Applied Physics Laboratory, The Johns Hopkins University, for the use of the radar records—a crucial part of the paper—and for his helpful discussions of their interpretation.

REFERENCES

Clarke, R. H., 1962: Pressure oscillations and fallout downdraughts. *Quart. J. Roy. Meteor. Soc.*, **88**, 459–469.

Drazin, P. G., 1958: The stability of a shear layer in an unbounded heterogeneous inviscid fluid. *J. Fluid Mech.*, **4**, 214–224.

——, and L. N. Howard, 1966: Hydrodynamic stability of parallel flow of inviscid fluid. *Advances in Applied Mechanics*, Vol. 9, New York, Academic Press, 1–89.

Eckart, C., 1960: *Hydrodynamics of Oceans and Atmospheres*. New York, Pergamon Press, 290 pp.

Emmanuel, C. B., B. R. Bean, L. G. McAllister and J. R. Pollard, 1972: Observations of Helmholtz waves in the lower atmosphere with an acoustic sounder. *J. Atmos. Sci.*, **29**, 886–892.

Goldstein, S., 1931: On the stability of superposed streams of fluid of different densities. *Proc. Roy. Soc. London*, **A132**, 524–548.

Gossard, E. E., and W. H. Munk, 1954: On waves in the atmosphere. *J. Meteor.*, **11**, 259–269.

——, J. H. Richter and D. Atlas, 1970: Internal waves in the atmosphere from high-resolution radar measurements. *J. Geophys. Res.*, **75**, 903–913.

Holmboe, J., 1960: Unpublished lecture notes (see Miles, 1963).

——, 1962: On the behavior of symmetric waves in stratified shear layers. *Geophys. Publ.*, **24**, No. 2, 67–113.

Hooke, W. H., F. F. Hall, Jr., and E. E. Gossard, 1973: Observed generation of an atmospheric gravity wave by shear instability in the mean flow of the planetary boundary layer. *Boundary Layer Meteor.*, **5**, 276–288.

Katz, I., 1972: The detection and study of gravity waves with microwave radar. *Proc. AGARD Conf. No. 115 on Effects of Atmospheric Acoustic Gravity Waves on Electromagnetic Wave Propagation*, 21-1 to 21-9.

Kelvin, Lord, 1880: On a disturbing infinity in Lord Rayleigh's solution for waves in a plane vortex stratum. *Nature*, **33**, 45–46.

Madden, T., and J. Claerbout, 1968: Jet stream-associated gravity waves and implications concerning jet stream instability. *Acoustic-Gravity Waves in the Atmosphere*, U. S. Govt. Printing Office, 121–134.

Miles, J. W., 1963: On the stability of heterogeneous shear flows. Part 2. *J. Fluid Mech.*, **16**, 209–227.

——, and L. N. Howard, 1964: Note on heterogeneous shear flow. *J. Fluid Mech.*, **20**, 331–336.

Ramm, Pauline, and F. W. G. Warren, 1963: Gravity-wave dispersion under wind shear in two model atmospheres. *Quart. J. Roy. Meteor. Soc.*, **89**, 349–359.

Rayleigh, J. W. S., 1945: *The Theory of Sound*, Vol. 2 (reprint of 2nd ed. of 1894). New York, Dover, Chap. 21.

Scorer, R. S., 1951: On the stability of stably stratified shearing layers. *Quart. J. Roy. Meteor. Soc.*, **77**, 76–84.

Sekera, Z., 1948: Helmholtz waves in a linear temperature field with vertical wind shear. *J. Meteor.*, **5**, 93–102.

Taylor, G. I., 1931: Effect of variation of density on the stability of superposed streams of fluid. *Proc. Roy. Soc. London*, **A132**, 499–523.

Tollmien, W., 1935: Ein allgemeines Kriterium der Instabilität Laminarer Geschwindigkeitsverteilungen. *Nachr. Ges. Wiss. Göttingen, Math.-Phys. Kl.*, **50**, 79–114 (translated as NACA, Tech. Memo., No. 792, 1936).